Non-invasive quantitative imaging of brain perfusion in hypocapnia by ASL MRI

Gonçalo Filipe Almeida Gomes [a*]

[a] *Dept. Bioengineering, IST, Lisbon, Portugal*
** goncalo.almeida.gomes@tecnico.ulisboa.pt*

ABSTRACT

Arterial Spin Labelling (ASL) is a Magnetic Resonance imaging (MRI) technique developed for the non-invasive, quantitative mapping of brain perfusion. In this work, the main goal was to optimize a kinetic modelling approach for quantitatively mapping brain perfusion using multiple post-labelling delay (PLD) ASL MRI acquisitions, during baseline and hypocapnia conditions.Multiple-PLD ASL data were collected on a 3T MRI system from twelve healthy volunteers. A pipeline for the analysis of the data was developed, including a number of pre-processing steps, followed by fitting of a General Kinetic Model for the estimation of CBF, BAT and aBV. Pre-processing included: motion correction and co-registration of the ASL images. Through the use of a saturation-recovery curve that was fitted to the control image it was possible to obtain a blood M_0 calibration value that was extracted from the estimated M_0 in CSF. For the model fitting, a Bayesian approach was employed.A statistical analysis was then performed to test for differences in the perfusion parameters between baseline and hypocapnia. The results showed a significant decrease in the grey matter mean value of CBF and the vascular mean value of aBV and a significant increase in the grey matter mean value of BAT, from baseline to hypocapnia, which is in agreement with the literature. In conclusion, the data analysis pipeline and kinetic modelling approach developed in this work were adequate. The use of ASL MRI to study perfusion changes in hypocapnia is very scarce in the literature, hence the importance of this study.

Keywords: Magnetic Resonance Imaging, Arterial Spin Labelling, Paced Deep Breathing, Brain Perfusion, Cerebral Blood Flow, Hypocapnia.

1. Introduction

In this section several aspects will be discussed: the main motivation for this work, then the physiological principles, the Arterial Spin Labelling technique and the state-of-the-art.

The brain is a crucial organ of the human body. Therefore, everything related to it is also important and worth studying. Brain perfusion or, in this case cerebral blood flow (CBF), is the process of delivering blood and nutrients to the capillary beds of the brain and it is always adjusting to the necessities of the brain. Furthermore, brain perfusion is also responsible for draining waste products from the tissue cells, like CO_2 and other metabolites. Hence, very important diagnostic information on status and functionality of brain tissues could be extracted from brain perfusion, allowing medical professionals to control patients with cerebral edema, traumatic brain injuries or stroke through the analysis of CBF.

Thus, given the importance of brain perfusion, it became clear that research of this brain characteristic was necessary and could be a great help for medical professionals. Cognitive tasks were developed to induce brain stimulation so that variations in CBF could be studied. These variations could be caused by a neurotransmitter release (Attwell & Iadecola, 2002), changes in oxygen at local levels or respiratory tasks (Ho et al., 2011).

So, in order to control and study the variations of brain perfusion to different stimuli, imaging techniques had to be devised to assess them, techniques like Arterial Spin Labelling (ASL) Magnetic Resonance Imaging.

1.1. Physiological Principles

CBF is usually measured in units of millilitres of blood per 100 grams of tissue per minute (ml/100g/min) (Buxton, 2002). It varies plenty within the human brain, depending on the type of tissue, where the average value of the grey matter is three times higher than white matter (Ito et al., 2004; Rostrup et al., 2005). However, it is established that the typical average value of CBF in the human brain is around 50-60 ml/100g/min (Buxton et al., 1998).

Hypocapnia is the decrease in arterial CO_2 partial pressure ($PaCO_2$) achieved by hyperventilation. With hyperventilation, the alveolar CO_2 concentration reduces which causes a decrease of the intravascular $PaCO_2$ and results in the increase of the perivascular and intra-neuronal pH, causing vasoconstriction and, therefore, CBF reduction (Posse et al., 1997). Hyperventilation also results in a mild increase in the oxygen arterial partial pressure (PaO_2), since the transport of oxygen to the lungs and arterial blood will be bigger (Bor-Seng-Shu et al., 2012). The hyperventilation is achieved using paced deep breathing techniques.

The other two parameters of interest, besides CBF, are the bolus arrival time (BAT) and the arterial blood volume (aBV). BAT is defined as the time it takes for the first molecule of labelled blood water to reach the first slice of the imaging region. aBV, is the arterial blood volume fraction, i.e., it is the percentage of intravascular arterial labelled water that is present in a certain voxel (Sousa et al., 2013).

1.2. Arterial Spin Labelling MRI

Nowadays, there is a relatively new and extremely interesting MRI technique for the measurement of blood perfusion, which is the Arterial Spin Labelling (ASL) (Alsop et al., 2014). This technique benefits from

the high abundance of water molecules in the human body and uses endogenous diffusible tracer, which in this case are the magnetically labelled blood water protons. This means that this technique is non-invasive and, therefore, can be repeated as long as needed per session. One other important characteristic is that ASL allows for the directly and quantitatively mapping of CBF changes.

The ASL technique has two main stages. The first stage is the labelling of arterial blood water molecules that end up in the imaging region, through the inversion or saturation of the longitudinal component of magnetization. This labelling is achieved using a RF pulse that is responsible for the inversion. The labelled blood, with time, flows into the imaging slices and eventually relaxes towards the equilibrium with the longitudinal relaxation time constant T_1 of blood. Then, after a certain interval, known as inversion time (TI), the magnetization is measured through the acquisition of an image with the slices of interest, that is called tag image or label image. This time delay allows for the labelled blood to reach the slices of the imaging region (Luh et al., 1999). The second stage is the acquisition of a second image, in the same slices of interest without the labelling process, i.e., there is no RF pulse. Here the blood is already fully relaxed and the image is known as the control image.

For the ASL technique to work, both the tag and control images have to be acquired. Typically the control image is acquired with a certain time interval from the tag image. This interval is called the repetition time, TR.

After the acquisition of both tag and control images, a subtraction of these two images is done in order to remove the contribution of the static tissue to the tag image, in which results a magnetization difference image (Equation 1). This image is roughly proportional to CBF at long acquisition times.

$$CBF \propto \Delta M = M_{control} - M_{tag} \quad (1)$$

One clear limitation of the ASL technique is the low Signal-to-Noise ratio (SNR), since the subtraction between the control and tag images leaves a magnetization difference around 1% of the total signal, which is less than the noise (Alsop et al., 2014). Therefore, one way of trying to get a better SNR is through averaging. Since the ASL is non-invasive and non-ionizing it is possible to repeat several times both the control and tag images, with a minimum TR between repetitions (Liu & Brown, 2007).

One way of labelling is the continuous labelling method (CASL) (Williams et al., 1992). Inside this method there are two distinct forms, the normal continuous ASL and the pseudo-continuous ASL (PCASL) (Dai et al., 2008). In the first one, it is applied one single, long label, typically 1 to 3s, in which an effective continuous RF pulse causes the inversion of the blood flowing through a single labelling plane. In the PCASL, a long train of slice-selective RF pulses (around 1000 at a rate of one per millisecond) replaces the continuous RF pulse applied at the labelling plane.

The other way of labelling is the pulsed labelling method (PASL) (Wong et al., 1997). This method requires the use of a single short RF pulse, normally with a duration of 10 to 20 ms that inverts a thick slab of tissue, including arterial blood water molecules. This slab, which constitutes the labelling bolus, is 10 to 20 cm thick because of the spatial coverage of the transmit RF coil. The duration of the pulse has to be very short, since the arterial blood water molecules, that are in the bolus, have high velocity flow (Alsop et al., 2014). In this work, the labelling method employed was the PASL.

1.3. State-of-the-Art

The CBF assessment in general has been successfully studied using several different methods, like ASL MRI.

Sousa et al. (2014) investigated the reproducibility of the CBF, BAT and aBV from arterial spin labelling data. One of the goals was also to test different estimation methods, like Bayesian inference methods, least squares fitting and a model-free approach. The average range of CBF was 45-59 ml/100g/min, 0.7-1.0 seconds for BAT and 0.35-1.17 % for aBV. In the conclusion, reproducible estimates of all three parameters was found using the Bayesian and least squares methods (Sousa et al., 2014).

As for the comparison of baseline versus hypocapnia, some studies address this issue, but not always to estimate the CBF. Like Sousa et al. (2014) that tested the reproducibility of the cerebrovascular reactivity using BOLD fMRI (functional MRI) when in hypocapnia caused by paced deep breathing. The results showed a good reproducibility of the hypocapnic CVR maps using PDB techniques (Sousa et al., 2014). Previously, another study revealed that PDB and consequently, hypocapnia, offers an alternative method for mapping the cerebrovascular reactivity, also using BOLD fMRI (Bright et al., 2009).

Thus, there are not many studies that assess the CBF during hypocapnia using ASL MRI, hence the interest of this work. However, it is quite common to assess the CBF during hypocapnia with other techniques. Like Ito et al. (2003) that used positron emission tomography and concluded that there was a decrease of the vascular blood velocity, since the degree of decrease of CBF in hypocapnia was greater than that of the CBV (Ito et al., 2003).

1.4. Thesis aims

The main goal of this thesis is to develop an appropriate kinetic modelling approach for the quantitative mapping of brain perfusion, bolus arrival time and arterial blood volume, based on multiple post-labelling delays (PLDs) ASL MRI acquisitions, during both baseline and hypocapnia conditions. Another important goal is to explore the parameters' priors in order to determine the optimal values, so that the model estimation can be efficient. In specific, the BAT prior is of highest interest due to the critical importance that this parameter has on the whole analysis and the high constringent that exists in this prior.

2. Materials and Methods

This section provides a detailed description of the materials and methods used in this work with the goal of estimating the parameters of interest and compare the two conditions. Two types of data were acquired, ASL and $P_{ET}CO_2$ data. It also includes the data analysis where several pre-processing stages were done, the model fitting used to estimate the parameters, with all its variants, in both conditions and the statistical analysis employed to assess the significance of the values obtained.

2.1. General Kinetic Model

The exact relationship between CBF and ΔM signal can be derived if this magnetization difference is handled as the concentration of a diffusible tracer (CBF tracer). In this condition, it is possible to apply appropriate tracer kinetic principles to estimate accurately the CBF, as well as BAT and aBV. The pulsed ASL signal of the tissue component

can be described by the General Kinetic Model taking the form of Equation 2 (Buxton et al., 1998; Chappell et al., 2010):

$$\Delta M_{tiss}(t) = \begin{cases} 0\,, & t < \Delta t \\ \dfrac{2\alpha M_{0a} f e^{-\frac{t}{T_{1app}}}}{R}\left(e^{Rt} - e^{R\Delta t}\right), & \Delta t \le t \le \Delta t + \tau \\ \dfrac{2\alpha M_{0a} f e^{-\frac{t}{T_{1app}}}}{R}\left(e^{R(\Delta t+\tau)} - e^{R\Delta t}\right), & \Delta t + \tau < t \end{cases} \quad (2)$$

where $R = \frac{1}{T_{1app}} - \frac{1}{T_{1a}}$ and $T_{1app} = \frac{1}{T_1} + \frac{f}{\lambda}$, f is the CBF, Δt is the BAT, M_{0a} is the equilibrium magnetization of the arterial blood, the τ is the bolus duration of the labelled blood bolus and α is the inversion efficiency, defined as the fraction of inversion of the arterial magnetization at the time of labelling (equal to 0.9). T_1 and T_{1a} are the tissue and arterial longitudinal relaxation time constants and the λ is the blood/tissue partition coefficient.

As mentioned several times before, the ASL signal may be contaminated by the labelled arterial blood in regions of larger vessels that are destined to regions that are more distal. Therefore, in some voxels that have a large arterial vessel, an extra component to the signal may appear from intravascular labelled water (macro-vascular signal). With this in mind, an extra macro-vascular component of the General Kinetic Model arises, that can be described by Equation 3 (Chappell et al., 2010):

$$\Delta M_{art}(t) = \begin{cases} 0\,, & t < \Delta t_a \\ 2\alpha M_{0a} e^{-\frac{t}{T_{1a}}} aBV\,, & \Delta t_a \le t \le \Delta t_a + \tau_a \\ 0\,, & \Delta t_a + \tau_a < t \end{cases} \quad (3)$$

where aBV is the arterial blood volume fraction, Δt_a and τ_a are the BAT and bolus duration of the arterial bolus. Theoretically, the BAT of the macro-vascular component should be shorter than the tissue component since the water molecules in the large vessels have greater velocity than that of the capillary beds.

Therefore, the total ASL signal from any voxel is the sum of the tissue and macro-vascular components (Equation 4):

$$\Delta \mathrm{M(t)} = \Delta M_{tiss}(t) + \Delta M_{art}(t) \quad (4)$$

Thus, through the General Kinetic Model (Equation 2 and 3) it is possible to estimate the CBF, BAT and aBV, but it necessary to sample the ASL signal across multiple post-labelling delays (PLDs), i.e., use several inversion times (TI) so that the fitting of the kinetic model allows for the estimation not only of CBF (for this, only one TI would be required), but also of the other parameters of interest (Chappell et al., 2010).

2.2. Parameter Estimation

For the parameter estimation the principle is to start with the ASL signal and obtain in the end the desired parameters (CBF, BAT, aBV). The method used for this was the probabilistic inference approach for nonlinear models (Chappell et al., 2009). This approach is based on the Bayes' theorem, which given the data y (in this case ASL signal, or ΔM) and the model $\mathcal{M}$ (General Kinetic Model), defines a posterior probability distribution function (PDF) for the model parameters w (Equation 5).

$$P(w|y,\mathcal{M}) = \frac{P(y,w|\mathcal{M})}{P(y|\mathcal{M})} = \frac{P(y|w,\mathcal{M})\,P(w|\mathcal{M})}{P(y|\mathcal{M})} \quad (5)$$

where $P(w|y,\mathcal{M})$ is the posterior probability of the parameters given the data and the model, $P(y|w,\mathcal{M})$ is the likelihood of the data given the model with parameters, $P(w|\mathcal{M})$ is the prior probability of the parameters for this model and the $P(y|\mathcal{M})$ is the evidence for the data given the model (Chappell et al., 2009).

Before estimating the parameters' values it was important to define what priors' values would be used. These were chosen according to the prior knowledge about the range of values that they might be likely to take. In Table 1 it is described the prior's values that were used in this work, in terms of the mean and variance of a normal distribution (Chappell et al., 2010).

Table 1 – Prior values for the parameters of the General Kinetic Model.

Parameter		Mean	Standard deviation
$\boldsymbol{f}$	(ml/g/s)	0	10^3
$\boldsymbol{\Delta t}$	(s)	0.7	0.3
$\boldsymbol{aBV}$	(%)	0	ARD
$\boldsymbol{\tau}$	(s)	0.75	0.3
$\boldsymbol{T_1}$	(s)	1.3	0.1
$\boldsymbol{T_{1a}}$	(s)	1.6	0.1
$\boldsymbol{\Delta t_a}$	(s)	0.5	0.3
$\boldsymbol{\tau_a}$	(s)	0.75	0.3

For CBF, a non-informative prior value was chosen, not having any prior assumptions about its value. More restrictive prior were chosen for the temporal parameters, like T_1 and T_{1a}, due to the knowledge of the actual physiological values (Chappell et al., 2010). The BAT prior was altered from the default values in order to see the importance of this prior and the optimized values for it

In most of the voxels there is no macro-vascular component in the signal, thus the fitting of three more parameters in tissue-only voxels might cause overfitting and consequently originating noise from artificial macro-vascular signal. So what was done was to use an automatic relevance determination (ARD) prior (Chappell et al., 2009) for the macro-vascular parameter (aBV). This method is very useful as it removes the macro-vascular component when not needed leaving only those voxels that really have this component. This allows the reduction of the model complexity from the data.

2.3. Data Acquisition

An initial group of 12 healthy subjects (6 males, age: 24,7 ± 2,5 years) was studied at Hospital da Luz. All the imaging acquisition was performed on a 3T Siemens Verio scanner using a 12-channel radio frequency coil.

The pulsed ASL data was acquired using a PICORE-Q2TIPS sequence, with Gradient-Echo EPI readout, repetition time (TR) of $2500\,ms$ and echo time (TE) of $19\,ms$ (one subject used $TE = 11\,ms$). The inversion times used (TI_2) varied from $400 - 2400\,ms$ in steps of $200\,ms$ with each control-tag pair repeated eight times, for averaging issues, yielding to 176 brain volumes. Another inversion time was acquired, $TI_2 = 50\,ms$, to be used in the off-resonance correction step. The voxel resolution used was 3.5 x 3.5 x 7.0 mm^3. For 7 of the subjects,

9 contiguous slices were acquired, yielding an image size of 64 x 64 x 9. For the rest of the subjects 28 contiguous slices were used, leaving the image size to be 64 x 64 x 28. These 7 subjects also had BOLD images acquired using a Gradient-Echo EPI sequence with $TR/TE = 2500/50\ ms$ and 110 brain volumes from 18 contiguous slices, yielding an image of 64 x 64 x 18 with a voxel resolution of 3.5 x 3.5 x 7.0 mm^3. A T_1-weighted structural image was obtained using an MPRAGE sequence, with $TR/TE = 2250/2.26\ ms$, 144 slices and voxel resolution of 1 x 1 x 1 mm^3.

During the entire experiment, the end-tidal carbon dioxide pressure ($P_{ET}CO_2$) of each exhalation was monitored using a capnograph (Cap10 Capnograph, Medlab GmbH) for eight of all subjects. The other four subjects had the end-tidal carbon dioxide pressure monitored through a CO_2 monitor (PN 8050. Dräger, Lübeck, Germany). Both methods used a nasal cannula that was connected to the capnograph and CO_2 monitor.

Subjects underwent two multi-PLD PASL acquisitions, one during REST and one during PDB. The total scan duration was approximately 15 minutes. In the REST acquisition the subjects did not receive any instruction. In the PDB periods the subjects were asked to breathe more intensely so as to increase the tidal volume while maintaining a steady head position. This is done by displaying visual instructions using stimulus presentation software, NORDIC NEURO LAB's Nordic fMRI solution (www.nordicneruolab.com). The whole task involves an alternating "inspire" and "expire", during PDB, with "breathe normally" instructions. The PDB period consists of 2 s of inspiration and 3 s expiration, which results in a breathing rate of 12 breaths/min (Sousa et al., 2014). With this task, the $PaCO_2$ will decrease, during paced deep breathing, which leads to hypocapnia and consequently CBF decrease, theoretically.

2.4. Data Analysis

For the analysis of the ASL data the tools available in FMRIB Software Library (FSL 5.0.8 version, http://fsl.fmrib.ox.ac.uk/fsl/fslwiki) (Jenkinson et al., 2012; Smith et al., 2004; Woolrich et al., 2009) were used, as well as in-house routines written in Matlab (version 2014b, http://mathworks.com). The essential analyses of this work were performed using FSL Bayesian Inference for Arterial Spin Labelling MRI (BASIL), among other tools used for all the pre-processing stages, image visualization and statistical analysis.

Motion Correction

Some precautions were taken in the image acquisition to ensure there was no head movement of the subject, since this is a relevant issue in any fMRI study. However, there is no guarantee that there was no movement, especially during the PDB task, which is more challenging for the subject. Therefore, a motion correction step was applied to the 4D ASL data, where the tool used for this purpose was the MCFLIRT tool (FMRIB's Motion Correction) (Jenkinson et al., 2002). The 4D ASL data consisted of the ASL time course from the REST condition combined with the ASL time course from the PDB condition. This way, the ASL data from REST and PDB conditions were aligned to each other, which is very useful in further steps.

The relative displacement is calculated relative to the previous time point. The motion correction reports for all subjects in the two conditions were then analyzed to see if there was a pattern that could be correlated between the conditions.

Image Registration

When performing fMRI studies, it is often useful to register the functional images (4D ASL data) to the structural (T_1-weighted structural image after brain extraction) and standard (MNI152 T_1-weighted image) space in order to enable comparisons. The structural space enables comparisons within a subject's brain between different areas and the standard space allows comparisons of different subject's brains. Therefore, it is obvious that registration is an essential step for multi-subject analysis. This image registration involves a transformation matrix that allows passing from the functional space to the structural or standard space.

In this work, the registration was done using the FMRIB's Linear Registration Tool (FLIRT) (Greve & Fischl, 2009; Jenkinson et al., 2002; Jenkinson & Smith, 2001) that creates the transformation matrix from one space to another if the images from the two spaces involved are given. Then it is possible to apply that transformation matrix to any image from the origin space so as to have that image in the space wanted.

Tag-Control Differencing

After the acquisition of the raw data for both conditions (REST and PDB), the control and tag images of each inversion time (TI) were merged together, yielding a 4D raw image with 176 volumes (for each of the 11 TI's, 16 volumes were acquired, 8 for tag and 8 for control).

Considering that control and tag images were acquired in an interleaved way, it was necessary to perform a subtraction of these images in order to obtain the magnetization difference image. There are several methods that can be used to obtain this ΔM image, like the pair-wise subtraction, the surround subtraction and the sinc subtraction (Liu & Brown, 2007). The simplest one and the one used in this work was the pair-wise subtraction. This method is the simple subtraction of adjacent images.

This pair-wise subtraction was performed using the *asl_file* command line tool of the FSL BASIL toolbox (Chappell et al., 2009). The averaging needed for better SNR was also done using this function, yielding the mean magnetization difference maps for each inversion time.

Off-Resonance Correction

The off-resonance correction is caused by an imperfect inversion slice profile, which happens due to a direct excitation of the labelling pulse in the imaging region. To estimate this effect, the magnetization difference map of the inversion time $TI_2 = 50\ ms$ was calculated, since at this early in the acquisition it was not expected that the imaging region already had labelled blood water molecules.

This way, the signal offset δM could be determined at each TI_2 acquired and at each slice, using the tissue time constant T_{1t} (Figueiredo et al., 2005):

$$\delta M(TI_2(z), z) = \delta M(TI_0, z) e^{-\frac{TI_2(z)+TI_0}{T_{1t}}} \quad (6)$$

where TI_0 is the $TI_2 = 50\ ms$ and $\delta M(TI_0, z)$ is the magnetization difference at TI_0 and specific z. Then it is only a matter of subtracting this signal offset, δM, to the acquired magnetization difference, ΔM_{acq}, in order to obtain the corrected magnetization difference image, ΔM_{corr}:

$$\Delta M_{corr}(TI_2(z), z) = \Delta M_{acq}(TI_2(z), z) - \delta M(TI_2(z), z) \quad (7)$$

This stage was performed using a Matlab routine that, by receiving the averaged magnetization difference map of all inversion times and the raw ASL data of the $TI_2 = 50\,ms$, outputted the corrected magnetization difference maps of each inversion time used for the posterior fitting.

Calibration

Knowing the value of the equilibrium magnetization of the arterial blood, M_{0a}, is essential for the parameter's estimations because otherwise, only relative values of the parameters would be saved and for the goals of this work, absolute values have to be estimated in order to enable the quantitative comparison.

The calibration method used was the Saturation Recovery. This method uses double in-plane pre-saturation pulses to saturate all the molecules, before the labelling takes place so that later the M_{0a} can be estimated from a M_0 image, like ASL control images.

Using Saturation Recovery, the signal from the calibration image can be expressed by the Equation 8 where $M(t)$ is the signal measured of the calibration image in the tissue of reference, in this case CSF, and M_{0t} is the equilibrium magnetization of that tissue. By inverting the following equation it was possible to recover M_{0t}. The tissue used in this analysis was the CSF because it is the tissue of the brain with the closest resemblance to blood in terms of number of water molecules:

$$M(t) = M_{0t}(1 - Ae^{\frac{-t}{T_{1t}}}) \quad (8)$$

where T_{1t} is the tissue time constant and A is a constant, normally 0.9. Then, M_{0a} can be estimated using the Equation 9.

$$M_{0a} = \lambda M_{0t} e^{TE(\frac{1}{T_{2t}^*} - \frac{1}{T_{2a}^*})} \quad (9)$$

where λ is the water partition coefficient of tissue-to-blood, where for the CSF is 0.87 (Herscovitch & Raichle, 1985), TE is the echo time of the sequence, ${T_{2t}}^*$ and ${T_{2a}}^*$ are the tissue of reference and arterial ${T_2}^*$, respectively. With M_{0a} calculated it is then possible to obtain the absolute values of the parameters of interest.

2.5. Model Fitting

With the priors defined, the model fitting could finally be done. This step was performed using the FSL command line tool *oxford*_asl from the BASIL toolbox.

An additional feature was used, the *spatial* prior (Groves et al., 2009) that uses adaptive spatial smoothness priors with a Gaussian kernel. It is directed only to the CBF image and is more or less similar to spatial smoothing the raw data. The main drawback of this approach is the blurring of the signal of interest, i.e., fine detail of a determined signal may be lost when applying the spatial prior. This is particularly relevant when the goal of the study is to analyse specific changes in certain anatomical regions and due to the spatial regularization, these changes may be lost.

Regions of Interest Definition

Then, three different regions of interest (ROI's) were created for the analysis of the parameters' values. The first one was a grey matter (GM) mask as the main focus of normal studies involving ASL MRI is this tissue.

The second ROI created was the Tissue mask. This mask was based on the previous one with an extra threshold. The 40% percentile of the REST CBF map of each subject was calculated and this value was used to threshold this same map within the GM mask in order to create the tissue mask. This mask was later used on both CBF and BAT maps of REST and PDB conditions.

The Vascular mask was the third ROI created. This mask was also based on the GM mask with an extra threshold. It was obtained by thresholding the REST aBV map above 10% of the mean for each subject, within the GM mask. This mask was then applied to the aBV maps of REST and PDB conditions.

Baseline vs Hypocapnia Comparison

The parameters' mean values of all subjects analysed were grouped together according to the parameter at question and the condition. This was done so that a group analysis could be done in order to compare the behaviour of the parameters from one condition to another.

When completed the group analysis, it was relevant to do a statistical analysis to infer if the conditions were statistically different or not, if the mean parameters' values had some kind of correlation with $P_{ET}CO_2$ data and if the parameters' maps of both conditions were themselves significantly different.

3. Results and Discussion

The following section describes the main results obtained in this work using the materials and methods presented in the previous chapter. First, the partial pressure of end-tidal carbon dioxide ($P_{ET}CO_2$) and the head movement results are presented. Next, the results of the perfusion parameters estimation are described. Then, the results of the group analysis of the two conditions, baseline and hypocapnia, are presented and the statistical analysis made.

3.1. End-Tidal Carbon Dioxide Pressure

The data was acquired in the form of time course with the $P_{ET}CO_2$ values. Then, a mean $P_{ET}CO_2$ value was calculated for each condition and is presented in Table 2, along with the values for the difference $P_{ET}CO_2$ (REST – PDB). For the subjects where the acquisition was performed with the CO_2 monitor (S6, S7, S8 and S9), only the difference values were available, as seen in Table 2.

Table 2 – $P_{ET}CO_2$ values in mmHg acquired in REST and PDB conditions, for every subject, also with the difference values. * denotes significant differences (p<0.05).

Subjects	$P_{ET}CO_2$ (mmHg)		Difference
	REST	PDB	
S1	14.05	6.08	7.97 *
S2	22.28	20.64	1.64 *
S3	21.53	16.95	4.58 *
S4	13.59	11.73	1.86 *
S5	18.20	15.47	2.73 *
S6			8.00
S7			3.80
S8			3.00
S9			2.70
S10	31.42	31.81	-0.40
S11	16.31	19.20	-2.88
S12	12.67	13.12	-0.45
Mean ± standard deviation	18.76 ± 6.2	16.88 ± 7.6	2.71 ± 3.2

The results show that, in general, there is a decrease of $P_{ET}CO_2$ from the REST condition to PDB, as expected. However, in subjects S10, S11 and S12 this decrease is not present (there is actually an increase in $P_{ET}CO_2$), which indicates that these subjects did not achieve hypocapnia when executing the task. Therefore, these subjects were discarded from this work, since the ASL MRI data from the PDB condition did not correspond to a subject performing hypocapnia. Figure 3.3 shows the bar charts of the

$P_{ET}CO_2$ values in REST and PDB for the subjects that had the $P_{ET}CO_2$ values from the REST and PDB recorded and actually performed hypocapnia.

For the subjects that had the $P_{ET}CO_2$ values from the REST and PDB recorded and actually performed hypocapnia, significant differences (paired t-test with equal variances, $p < 0.05$) were found between REST and PDB condition. Another aspect worth mentioning is that $P_{ET}CO_2$ values vary across subjects, which may be due to different respiratory activity across subjects and/or to differences in the calibration of the CO2 measurement setup. In any case, in this work, as long as a decrease from REST to PDB is present, this should not make a difference.

The subjects used for the rest of this work were S1, S2, S3, S4, S5, S6, S7, S8 and S9.

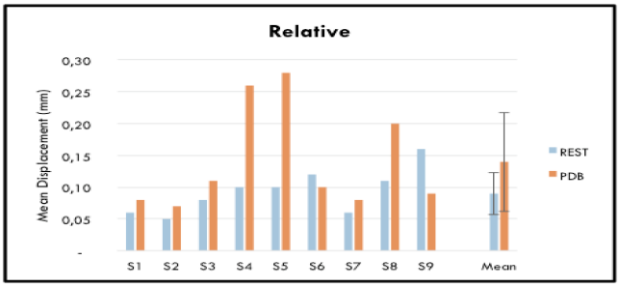

Figure 1 – Mean displacement in mm bar charts for the subjects analysed, with absolute values (left) and relative values (right). Error bars represent the standard deviation of the mean.

3.2. Head Motion

The volumes of each ASL acquisition time series were re-aligned yielding the mean relative displacement values for each subject (Figure 1).

From these results, it is clear that, in general, the acquisitions made in PDB condition have more head movement than the acquisitions in REST condition. This is interesting as it shows that maybe there is some struggle to the subject associated with performing the PDB task. No significant differences were found (paired t-test with equal variances, $p < 0.05$) between REST and PDB condition. However, a p-value of 0.078 was reached which is not that far from significant difference.

Another important aspect is that there are some subjects that have very high displacement in a determined condition when compared with the other, like S4, S5, S8 and S9. However, this increase in the mean displacement in a specific condition is localised, i.e., it is not a general head movement along the entire acquisition. Therefore, one option was to remove the volumes that corresponded to this local movement, yet, it required many volumes to which without them the model fitting would be ruined. Another option was to remove these subjects from the analysis but since there were already few subjects that would lead to a less significant group analysis.

Therefore, for all subjects, motion correction was performed with the intent to minimize these head movements.

3.3. Parameters' Prior Distribution

BAT prior

The main modifications to the BAT prior were in the mean where 0.6 s, 0.7 s (default) and 0.8 s were tested and in the standard deviation of the mean where 0.1 s, 0.3 s (default), 0.5 s, 1 s and 10^4 s were examined.

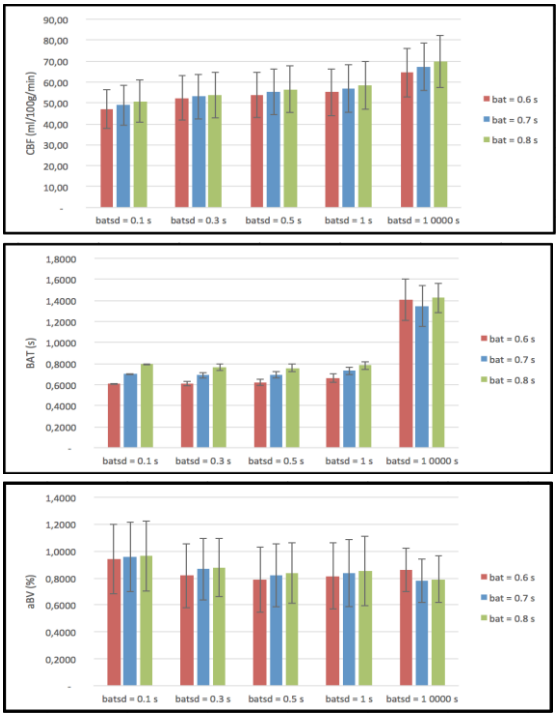

Figure 2 – Bar charts for CBF (top), BAT (middle) and aBV (bottom) values for each combination of BAT prior. Error bars represent the standard deviation of the mean values.

Since the goal of this analysis was to check what the optimized values were for the BAT prior, only the acquisitions from REST condition were analysed, for simplicity reasons. In Figure 2 the three parameters' estimations for each combination of mean and standard deviation of BAT prior used are presented. The values presented in that table represent the parameters values averaged for all subject in REST condition within each combination of BAT prior, where the average was performed in the GM ROI mask without the *spatial* prior and in the functional (native) space.

Several aspects can be concluded from Figure 2. The increase in the standard deviation of the BAT prior (*batsd*) causes an increase in CBF possibly due to a growth of deceiving fitting voxels that have wrong estimates. For the aBV parameter the opposite effect is verified. With this *batsd* increase, the BAT parameter suffers a general increase caused by the direct expansion of the standard deviation of the prior, which allows a greater range of estimate values. However, the same effect of wrong fitting voxels is also observed more intensively in this parameter as it is perceived when *batsd* = 10^4 s, i.e., by removing the BAT prior information.

With these results it was decided to use *bat* = 0.7 s and *batsd* = 0.5 s for the next analyses. This way it is possible to have a greater range of estimation values for BAT.

Spatial Prior

The next step in this work was to see whether or not, to use the *spatial* prior for the model fitting. Then, for the subjects analysed two estimations were made for each parameter of interest with and without the *spatial* prior. Figure 3 shows the maps for the CBF parameter with and without *spatial* prior for subject S2 in a specific slice.

The CBF mean value estimated averaged across all subjects with and without the *spatial* prior was 41.86 and 55.28 ml/100g/min, respectively. The main conclusion for the CBF parameter is that using *spatial* prior decreases the mean value estimated as expected considering that through the spatial prior neighbouring voxels are contemplated, which reduces the value of certain voxels.

The benefits of using the *spatial* prior are that the model fitting produces more accurate estimation overall, however some local resolution is lost, which could be a problem when searching for a specific region in the brain. Nonetheless, for the rest of the work it was decided to use the *spatial* prior.

3.4. Parameters' Values and Group Analysis

The results of the group analyses are presented now. First, the parameters' mean values estimates and maps for the GM ROI mask, then for the Tissue and Vascular ROI masks For all these analyses a simple paired t-test with equal variances ($p < 0.05$) was also made comparing the REST and PDB conditions.

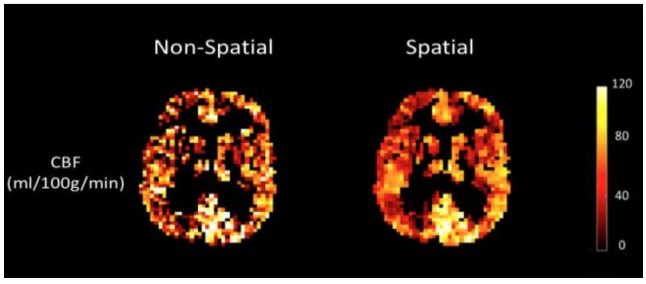

Figure 3 – CBF map for subject S2 with and without *spatial* prior.

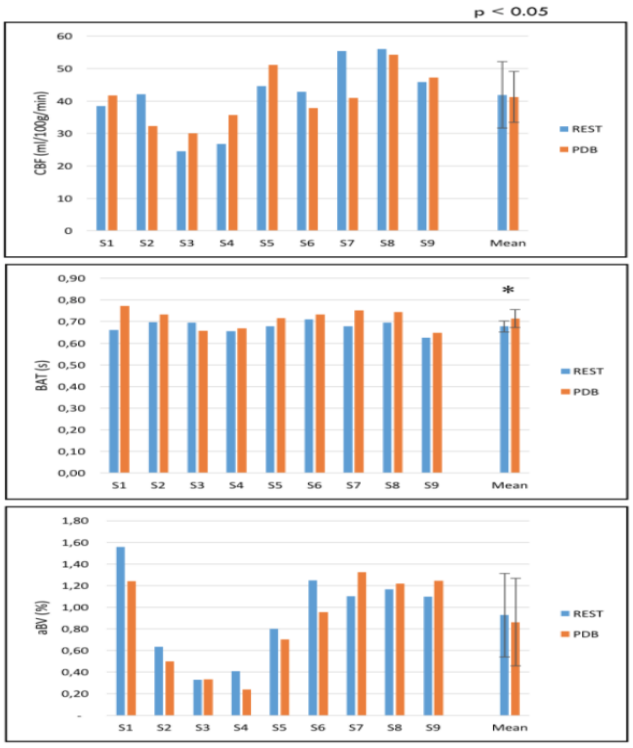

Figure 4 – Bar charts of CBF, BAT and aBV maps for all subjects in REST and PDB, using GM ROI mask. Error bars represent the standard deviation of the mean values and * denotes significant differences (p<0.05).

Grey Matter ROI Mask

The comparison between the baseline and hypocapnia condition was done through the study of the three parameters of interest, CBF, BAT and aBV. The model fitting performed estimated these parameters maps for each condition. Therefore, it was possible to obtain the mean values of these maps. These were calculated in the Grey Matter ROI mask. Figure 4 presents these mean values obtained for each subject and each condition in the form of bar charts.

The results above show that for CBF, in general, there is a small decrease in the subjects' mean from REST to PDB. However, this is not significantly different as five of the subjects actually suffer an increase in the mean value. In theory, when performing hypocapnia there should be a decrease in brain perfusion due to the vasoconstriction that takes place, so overall the results are in agreement with this.

For BAT, it is observed that, in general, there is an increase in the subject's mean values from REST to PDB (only subject S3 showed a decrease). This is also in agreement with the theory and literature as with vasoconstriction and decrease in brain perfusion the labelled blood takes more time to reach the imaging region and consequently increasing the BAT. For this parameter, significant differences were found between REST and PDB, which supports its behaviour.

In hypocapnia, theoretically, the blood vessels should have smaller sizes due to the vasoconstriction that occurs. Therefore, the aBV should decrease in PDB when compared with REST, which is exactly what happens for almost all subjects (only S3, S7, S8 and S9 showed the opposite). Therefore, in general the model fitting is again in agreement with the literature and theory. However, in this case and similar to CBF, no significant differences were found between REST and PDB.

From Figure 4 it is possible to see that the CBF, BAT and aBV values themselves are in agreement with the literature where CBF is in the range of 40 – 60 ml/100g/min, BAT is around 0.7 s and aBV is approximately 0.5 to 1.5 % (Chappell et al., 2010; Sousa et al., 2013).

It is worth mentioning that in all three parameters the subjects S2, S3, S4 and S5 show, overall, lower mean values, which is interesting as these are the subjects for which the data acquired had 28 slices instead of 9 like for the other subjects. Hence, this could mean that the more superior and inferior regions of the brain (present in the subjects with 28 slices) cause for the mean values to decrease.

Figure 6 shows the CBF, BAT and aBV maps for subject S2 in REST and PDB conditions. In Figure 6 (top) it is possible to see that, in general, there is more brain perfusion in voxels from the inferior and posterior region. This area corresponds to the occipital lobe that is responsible for all the visual processing. The reason for this brain perfusion behaviour is because the subject's eyes had to be open due to the presentation of visual cues of the task.

The aBV parameter maps are very different from the CBF and BAT maps since almost all aBV signal is present in either the middle of the brain or in the lateral cerebral cortex. The Circle of Willis is located at the basis of the brain and is where the internal carotid arteries end and from where the anterior and posterior cerebral arteries begin, which explains the signal from the middle of the brain. The signal from the lateral cerebral cortex is explained with both left and right middle cerebral arteries (MCA) that supply blood to this area.

Despite the mean values obtained, it is possible to see from Figure 6 (top) that subject S2 has a clear decrease of brain perfusion from REST to PDB, i.e., there is a decrease of CBF and aBV and an increase of BAT, which is the expected.

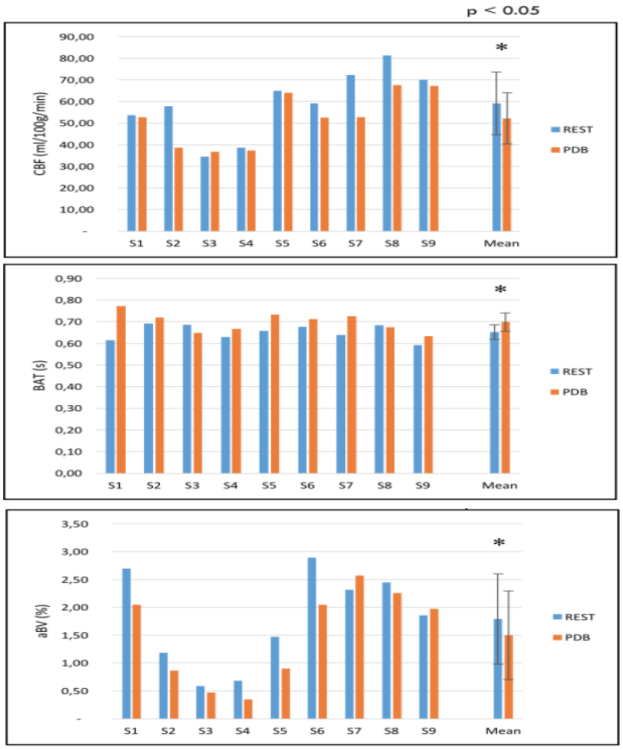

Figure 5 – Bar charts of CBF, BAT and aBV maps for all subjects in REST and PDB, using Tissue and Vascular ROI masks. Error bars represent the standard deviation of the mean values and * denotes significant differences (p<0.05).

Tissue and Vascular ROI Masks

In this case all the parameters' maps mean values were calculated in the Tissue and Vascular ROI masks. Figure 5 shows these results obtained for each subject and each condition in the form of bar charts.

For CBF all the mean values have increased when compared with the results from the previous section, which is expected since only the 40% percentile is considered in this mask. Besides, only one subject (S3) did not have the decrease from REST to PDB, which is a clear improvement from the previous section.

The Tissue mask does not have any threshold on the BAT parameter, however this mask is also used when obtaining the mean values of this parameter maps, so it is possible that some changes could be verified when comparing to the results from GM mask. This is actually the case as, overall, there is a decrease in these values using the Tissue mask. Subjects S3 and S8 showed a decrease from REST to PDB. Nonetheless, this is a not so good result as in the previous section, where only subject S3 had this decrease.

For aBV a similar behaviour as CBF takes place, since the Vascular mask applies a threshold in this parameter (as described in section 2.2.3). Hence, for aBV an increase in the mean values is also observed, using this mask. There is also an improvement in this mask since now only subjects S7 and S9 showed an increase from REST to PDB, which are fewer subjects than the results from the previous section.

With these Tissue and Vascular masks, the most important aspect that changes relative to the results from the previous section is the fact that now all three parameters are significantly different between REST and PDB. Therefore, these results are, in theory, better than the previous ones and demonstrate that the model fitting used is adequate for this type of data.

The same aspects verified in the previous section maps are still present in the ones from Figure 6 (bottom), i.e., the occipital lobe still has an enhanced brain perfusion and the aBV signal is still present, almost exclusively, in the MCA area.

The maps from Figure 6 (bottom) show that, when comparing with the maps from GM ROI mask, the same changes from REST to PDB are verified, i.e., the decrease of CBF and aBV and the increase of BAT, but with more significance

In general, the results obtained with Tissue and Vascular ROI masks are better than the ones with GM ROI mask, so for the next analysis the first masks will be used.

3.5. Statistical Analysis

Correlation with $P_{ET}CO_2$

The results of the correlation between the parameters and the $P_{ET}CO_2$ in both REST and PDB conditions are now presented. More precisely, the parameters' maps mean values of PDB were subtracted to these values of REST condition for each subject, yielding ΔCBF, ΔBAT and ΔaBV. Then, these differenced values were correlated with the differenced $P_{ET}CO_2$ (REST – PDB), $\Delta P_{ET}CO_2$, again for each subject. This process was done for both GM ROI mask and Tissue and Vascular ROI masks. The correlation coefficients and respective p-value (paired t-test, $p < 0.05$) for each parameter are presented in Table 3.

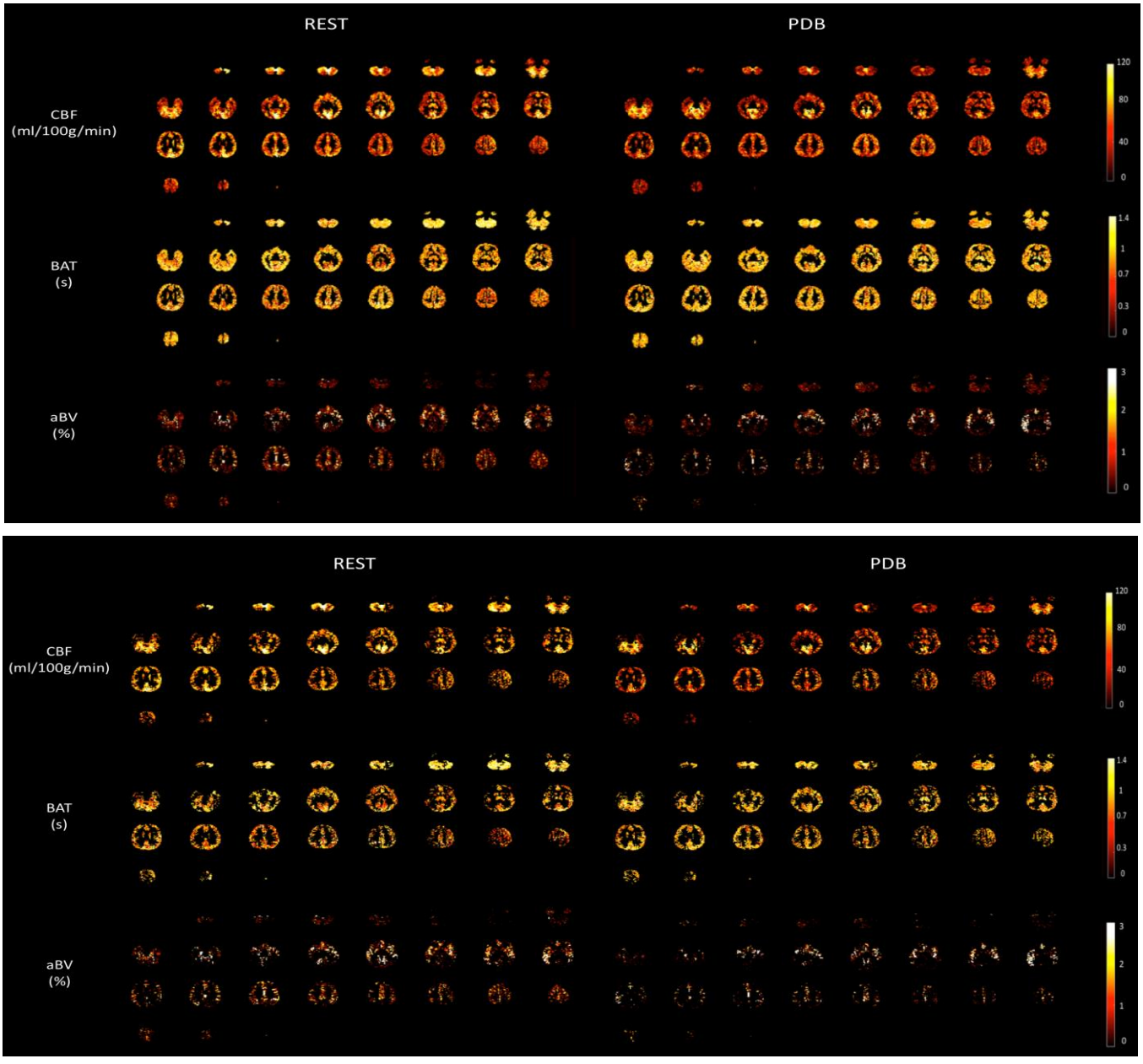

Figure 6 – CBF, BAT and aBV maps for subjects S2 in GM ROI mask (top) and in Tissue and Vascular ROI masks (bottom).

Theoretically, the greater the $\Delta P_{ET}CO_2$ the greater the ΔCBF and ΔaBV should be, because the more hypocapnia the subject experiences, the less brain perfusion and more vasoconstriction happens in the brain, leading to a decrease in both CBF and aBV. For ΔBAT this relationship is inverted, i.e., the more hypocapnia, the greater the time it takes for the labelled blood to reach the imaging region, consequence of the vasoconstriction and less brain perfusion. Therefore, in theory, for CBF and aBV there should be a positive correlation with $P_{ET}CO_2$ and for BAT a negative one.

The results obtained show that for GM ROI mask all three parameters are in agreement with the theory, yet the CBF correlation coefficient is very small, exhibiting that the correlation is not very strong. For the Tissue and Vascular ROI masks, CBF loses the little correlation that the previous mask had but BAT and aBV show an improvement in the correlation observed when compared with the GM ROI mask. For neither of the masks used significant differences were reached between the differenced parameters values and $\Delta P_{ET}CO_2$.

Table 3 – Correlation coefficients and p-values for each parameter and in both GM mask and Tissue/Vascular masks.

Parameters	GM ROI Mask		Tissue/Vascular ROI Masks	
	Correlation coefficient	p-value	Correlation coefficient	p-value
CBF	0.033	0.932	-0.270	0.482
BAT	-0.314	0.410	-0.388	0.302
aBV	0.509	0.161	0.545	0.129

There are several possibilities to explain these results obtained. The main reason is that each subject has its own characteristic respiratory activity, which despite having a greater $\Delta P_{ET}CO_2$ does not necessarily mean that the subject is performing real hypocapnia. Another possible reason is the head movement that the subject had, that could have biased the model fitting and consequently the parameters' estimations.

4. Conclusions

In summary, this work explored the behaviour of the brain perfusion when subjected to a hypocapnia task, investigating the best ways to estimate the perfusion and arterial parameters and examining the masks to be used for the estimations, as well as the study of the statistical analysis. Therefore, an appropriate kinetic modelling approach for the quantitative mapping of brain perfusion, bolus arrival time and blood volume was developed, using multi-TI ASL MRI acquisitions during baseline and hypocapnia conditions.

An important effect of the distribution of the BAT prior on the variability of the BAT estimates was found, and it was concluded that a relatively larger prior should be used if significant changes in the BAT parameter are to be found. This is particularly critical in hypocapnia, since the decreased blood flow in this case is expected to prolong the arterial transit time and hence increase BAT.

Overall, the model fitting developed was adequate and with the macro-vascular component, it was possible to isolate the intra-vascular signal (aBV), yielding a brain perfusion signal more or less free of contamination from large blood vessels. This extra component creates an alternative for the flow-suppression techniques which may limit the already very low SNR of the data. In general the Bayesian model fitting method used here seems to provide a good alternative to standard least squares methods, provided that care is taken in the definition of the parameters priors according to the study of interest.

The group analysis results obtained in this work showed a characteristic behaviour of brain perfusion while the subject is experiencing hypocapnia, when compared with the baseline condition. In general, when in hypocapnia, CBF and aBV suffer a decrease and BAT an increase. This was expected, as hypocapnia leads to vasoconstriction causing a decrease in blood perfusion, which in turn lengthens the time it takes for the labelled blood to reach the imaging region (hence increasing BAT) and the decreases the arterial blood volume (hence decreasing aBV).

These changes were significant within the Tissue and Vascular ROIs defined based on the CBF and aBV results at rest, respectively. The CBF decrease was however not significant in an anatomically defined GM ROI, which probably reflects a poor SNR and consequently poor model fitting, leading to limited sensitivity. Such limited sensitivity of our data may also explain the lack of significant differences over the whole brain in our voxel-wise comparison between hypocapnia and rest conditions. Nevertheless, some brain regions did show significant effects, if uncorrected for multiple comparisons.

In order to improve the study's sensitivity, more subjects should be used. Moreover, because the $P_{ET}CO_2$ results excluded some subjects that did not show hypocapnia despite performing the task, perhaps some modifications should be made to the paced deep breathing paradigm so that it could be guaranteed that the subject is achieving hypocapnia. It also became clear that in hypocapnia there is a greater amount of head movement, which dampers the ASL MRI signal. This was verified through the head mean displacement results, as well as the number of bad fitting voxels, which reflected the difficulty of the model fitting in correctly estimating the parameters when the subject is performing hypocapnia.

Further research should be made to attenuate the low SNR and its relevance. The paced deep breathing task itself should be improved in order to guarantee that the subjects are performing hypocapnia and not moving at all (so that there is no head motion). Also, so as to reduce the intra-subject variability of the $P_{ET}CO_2$ results, a more careful regulation of the rate and depth of the subjects breathing should be done. Further research about the masks and thresholds to be used should be made as the results obtained with these are far from optimal and there are several different possibilities to account. Likewise, for the several options that the FSL BASIL toolbox offers. It is also essential to increase the number of subjects in the study in order to have a more representative group analysis.

Acknowledgements

A note of gratitude goes to Prof. Patrícia Figueiredo, who supervised this work, to all the people from the NeuroPhysim project who acquired and provided the data for this study. A special thanks to Joana Pinto for all the shared knowledge, the availability and the algorithms that she kindly provided.

References

Alsop, D. C., Detre, J. a., Golay, X., Günther, M., Hendrikse, J., Hernandez-Garcia, L., & Zaharchuk, G. (2014). Recommended implementation of arterial spin-labeled perfusion MRI for clinical applications: A consensus of the ISMRM perfusion study group and the european consortium for ASL in dementia. *Magnetic Resonance in Medicine*, *00*(October 2013).

Attwell, D., & Iadecola, C. (2002). The neural basis of functional brain imaging signals. *Trends in Neurosciences*.

Bor-Seng-Shu, E., Kita, W. S., Figueiredo, E. G., Paiva, W. S., Fonoff, E. T., Teixeira, M. J., & Panerai, R. B. (2012). Cerebral hemodynamics: concepts of clinical importance. *Arquivos de Neuro-Psiquiatria*, *70*(5), 352–356.

Bright, M. G., Bulte, D. P., Jezzard, P., & Duyn, J. H. (2009). Characterization of regional heterogeneity in cerebrovascular reactivity dynamics using novel hypocapnia task and BOLD fMRI. *NeuroImage*, *48*(1), 166–175.

Buxton, R. B. (2002). Introduction to Functional Magnetic Resonance Imaging: Principles and Techniques. *Energy*, *24*(2), xi, 523 p.

Buxton, R. B., Frank, L. R., Wong, E. C., Siewert, B., Warach, S., & Edelman, R. R. (1998). A general kinetic model for quantitative perfusion imaging with arterial spin labeling. *Magnetic Resonance in Medicine : Official Journal of the Society of Magnetic Resonance in Medicine*, *40*(3), 383–396.

Chappell, M. a., Groves, a. R., Whitcher, B., & Woolrich, M. W. (2009). Variational Bayesian Inference for a Nonlinear Forward Model. *IEEE Transactions on Signal Processing*, *57*(1), 223–236. http://doi.org/10.1109/TSP.2008.2005752

Chappell, M. a., MacIntosh, B. J., Donahue, M. J., Günther, M., Jezzard, P., & Woolrich, M. W. (2010). Separation of macrovascular signal in multi-inversion time arterial spin labelling MRI. *Magnetic Resonance in Medicine*, *63*(5), 1357–1365.

Chappell, M. a., Woolrich, M. W., Petersen, E. T., Golay, X., & Payne, S. J. (2013). Comparing model-based and model-free analysis methods for QUASAR arterial spin labeling perfusion quantification. *Magnetic Resonance in Medicine*, *69*(5), 1466–1475.

Dai, W., Garcia, D., De Bazelaire, C., & Alsop, D. C. (2008). Continuous flow-driven inversion for arterial spin labeling using pulsed radio frequency and gradient fields. *Magnetic Resonance in Medicine*, *60*(6), 1488–1497.

Figueiredo, P. M., Clare, S., & Jezzard, P. (2005). Quantitative perfusion measurements using pulsed arterial spin labeling: Effects of large region-of-interest analysis. *Journal of Magnetic Resonance Imaging*, *21*(6), 676–682.

Greve, D. N., & Fischl, B. (2009). Accurate and robust brain image alignment using boundary-based registration. *NeuroImage*, *48*(1), 63–72.

Groves, A. R., Chappell, M. A., & Woolrich, M. W. (2009). Combined spatial and non-spatial prior for inference on MRI time-series. *NeuroImage*, *45*(3), 795–809.

Herscovitch, P., & Raichle, M. E. (1985). What is the correct value for the brain--blood partition coefficient for water? *Journal of Cerebral Blood Flow and Metabolism : Official Journal of the International Society of Cerebral Blood Flow and Metabolism*, *5*(1), 65–69.

Ho, Y.C. L., Petersen, E. T., Zimine, I., & Golay, X. (2011). Similarities and differences in arterial responses to hypercapnia and visual stimulation. *Journal of Cerebral Blood Flow and Metabolism : Official Journal of the International Society of Cerebral Blood Flow and Metabolism*, *31*(2), 560–571.

Ito, H., Kanno, I., Ibaraki, M., Hatazawa, J., & Miura, S. (2003). Changes in human cerebral blood flow and cerebral blood volume during hypercapnia and hypocapnia measured by positron emission tomography. *J Cereb Blood Flow Metab*, *23*(6), 665–670.

Ito, H., Kanno, I., Kato, C., Sasaki, T., Ishii, K., Ouchi, Y., & Senda, M. (2004). Database of normal human cerebral blood flow, cerebral blood volume, cerebral oxygen extraction fraction and cerebral metabolic rate of oxygen measured by positron emission tomography with 15 O-labelled carbon dioxide or water, carbon monoxide and oxygen: *European Journal of Nuclear Medicine and Molecular Imaging*, *31*(5), 635–643.

Jenkinson, M., Bannister, P., Brady, M., & Smith, S. M. (2002). Improved optimisation for the robust and accurate linear registration and motion correction of brain images. *NeuroImage*, *17*, 825–841.

Jenkinson, M., Beckmann, C. F., Behrens, T. E. J., Woolrich, M. W., & Smith, S. M. (2012). FSL. *NeuroImage*.

Jenkinson, M., & Smith, S. (2001). A global optimisation method for robust affine registration of brain images. *Medical Image Analysis*, *5*(2), 143–156.

Liu, T. T., & Brown, G. G. (2007). Measurement of cerebral perfusion with arterial spin labeling: Part 1. Methods. *Journal of the International Neuropsychological Society : JINS*, *13*(3), 517–525.

Luh, W., Luh, W., Wong, E. C., Wong, E. C., Bandettini, P. a, Bandettini, P. a, & Hyde, J. S. (1999). QUIPSS II With Thin-Slice TI 1 Periodic Saturation: A Method for Improving Accuracy of Quantitative Perfusion Imaging Using Pulsed Arterial Spin Labeling. *Magnetic Resonance in Medicine*, *1254*, 1246–1254.

Posse, S., Olthoff, U., Weckesser, M., Jäncke, L., Müller-Gärtner, H. W., & Dager, S. R. (1997). Regional dynamic signal changes during controlled hyperventilation assessed with blood oxygen level-dependent functional MR imaging. *American Journal of Neuroradiology*, *18*(9), 1763–1770.

Rostrup, E., Knudsen, G. M., Law, I., Holm, S., Larsson, H. B. W., & Paulson, O. B. (2005). The relationship between cerebral blood flow and volume in humans. *NeuroImage*, *24*(1), 1–11.

Smith, S. M., Smith, S. M., Jenkinson, M., Jenkinson, M., Woolrich, M. W., Woolrich, M. W., & Matthews, P. M. (2004). Advances in functional and structural MR image analysis and implementation as FSL. *NeuroImage*, *23 Suppl 1*, S208–19.

Sousa, I., Vilela, P., & Figueiredo, P. (2013). Reproducibility of the quantification of arterial and tissue contributions in multiple postlabeling delay arterial spin labeling. *Journal of Magnetic Resonance Imaging*, *1462*, 1453–1462.

Sousa, I., Vilela, P., & Figueiredo, P. (2014). Reproducibility of hypocapnic cerebrovascular reactivity measurements using BOLD fMRI in combination with a paced deep breathing task. *NeuroImage*, *98*, 31–41.

Williams, D. S., Detre, J. A., Leigh, J. S., & Koretsky, A. P. (1992). Magnetic resonance imaging of perfusion using spin inversion of arterial water. *Proceedings of the National Academy of Sciences of the United States of America*, *89*(1), 212–216.

Wong, E. C., Buxton, R. B., & Frank, L. R. (1997). Implementation of quantitative perfusion imaging techniques for functional brain mapping using pulsed arterial spin labeling. *NMR in Biomedicine*, *10*(4-5), 237–49.

Woolrich, M. W., Jbabdi, S., Patenaude, B., Chappell, M., Makni, S., Behrens, T., & Smith, S. M. (2009). Bayesian analysis of neuroimaging data in FSL. *NeuroImage*, *45*, S173–186.